Cascarano *et al.* (1982) that the S&R results only apply to an experiment carried out with both wavelengths at the high-frequency side of the absorption edge is erroneous.

For acentric reflections the S&R method is more flexible than the ratio technique since it offers the possibility of using relative scaling schemes other than (16).

References

BARTUNIK, H. D. (1978). *Acta Cryst.* A**34**, 747-750.

CASCARANO, G., GIACOVAZZO, C., PEERDEMAN, A. F. & KROON, J. (1982). *Acta Cryst.* A**38**, 710-720.

HELLIWELL, J. R. (1984). *Rep. Prog. Phys.* **47**, 1403-1497.

HOSAYA, S. (1975). *Anomalous Scattering*, edited by S. RAMASESHAN & S. C. ABRAHAMS, pp. 275-287. Copenhagen: Munksgaard.

KLOP, E. A., KRABBENDAM, H. & KROON, J. (1989). *Acta Cryst.* A**45**, 203-208.

RAMASESHAN, S. & NARAYAN, R. (1981). *Structural Studies on Molecules of Biological Interest*, edited by G. G. DODSON, J. P. GLUSKER & D. SAYRE, pp. 233-245. Oxford: Clarendon Press.

SAKAMAKI, T., HOSAYA, S. & FUKAMACHI, T. (1980). *Acta Cryst.* A**36**, 183-189.

SAKAMAKI, T., HOSAYA, S., TAGAI, T., OHSUMI, K. & SATOW, Y. (1984). *J. Appl. Cryst.* **17**, 219-225.

SINGH, A. K. & RAMASESHAN, S. (1968). *Acta Cryst.* B**24**, 35-40.

UNANGST, D., MÜLLER, E., MÜLLER, J. & KEINERT, B. (1967). *Acta Cryst.* **23**, 898-901.

WOOLFSON, M. M. (1984). *Acta Cryst.* A**40**, 32-34.

Acta Cryst. (1989). A**45**, 613-620

The Relation of Scan Range and Reflection Shape in Single-Crystal 1D Profile Measurement

BY A. MCL. MATHIESON

Chemistry Department, La Trobe University, Bundoora, Victoria, Australia, 3083

(*Received* 19 *December* 1988; *accepted* 29 *March* 1989)

Abstract

Changes in shape of 1D profiles of small-single-crystal Bragg reflections have been examined in terms of the shapes of the components which, convoluted together, generate the profile. In most practical cases, operational features require truncation of the angular scan range of measurement and the conventional linear formula for scan range, $\omega = a + b \tan\theta$, is then not strictly valid. A more appropriate relationship involves a combination of root mean square (RMS) and linear (LIN) forms,

$$\omega = [(p')^2 + (q' \tan\theta)^2]^{1/2} + (p'' + q'' \tan\theta)$$

where p' is associated with the leading and trailing edges of the distribution of the combined θ-invariant components and p'' with its plateau width while q' is associated with the leading and trailing edges of the distribution of the wavelength component and q'' with the separation of its outer peaks if there are more than one. For operational purposes, this relationship can be substituted with adequate precision by $\omega = [c^2 + (d \tan\theta)^2]^{1/2}$, but the parameters c and d do not then have a simple relationship to the θ-invariant and θ-variant components. Use of a conventional linear formula when a RMS one is the relevant one can mean that, in the lower θ range, the estimate of integrated intensity will be too high and, in the higher θ range, it will be too low, so that, with increasing θ, a positive then a negative systematic error is introduced and not merely a negative error as the conventional interpretation of truncation holds. The conclusions of the present analysis are tested against experimental data where the conventional treatment for truncation failed [Eisenstein & Hirshfeld (1983). *Acta Cryst.* B**39**, 61-75]. For the estimation of integrated intensity, and hence of structure factors, which are consistent over the operational range of θ, a RMS formula for the scan range is advisable.

Introduction

Diffractometry of a small single crystal involves measurement of a large number of Bragg reflections distributed over a wide range of scattering angle, θ. To ensure that these reflections are placed on a mutually consistent and therefore directly comparable basis, the measurements for each reflection should be carried out over an exactly equivalent region of diffraction space, determined by the angular ranges of the respective contributing components (Mathieson & Stevenson, 1985). If one wishes to ensure that this condition is truly satisfied, then 2D measurements in $\Delta\omega$, $\Delta 2\theta$ space have the advantage that the appropriate region can be defined readily.

Until position-sensitive detectors with an authentic resolution of (say) 50 μm are commonly available to facilitate 2D data collection of individual Bragg reflections in diffraction space, it is likely that the majority of crystal structure studies will continue to be effected using 1D measurement of the counter profile varying ω. As one moves from reflection to reflection, this involves adjusting the scan range [and the detector aperture, except in the case of the $\omega/2\theta$ scan mode (Mathieson, 1983)] in some systematic

0108-7673/89/090613-08$03.00

way to ensure that the consistency condition holds, within the intrinsic limitations of 1D measurement (Mathieson, 1984*a*).

The formula which has been customarily used to determine the size of the scan range under these circumstances is the linear (LIN) form, $\omega = a + b \tan\theta$ (*e.g.* Arndt & Willis, 1966; Clegg, 1984). The first term allows for the contributions of components which are θ-invariant, such as the source size and crystal specimen mosaic distribution (if isotropic), while the second term allows for the effect of wavelength dispersion. Numerical values of a and b used in practice by crystallographers often owe more to perceived traditional wisdom than to experimental exploration; see, however, a recent empirical study by Destro & Marsh (1987) and also Destro (1988).

Recently, following studies of profile shape by Höche, Schulz, Weber, Belzner, Wolf & Wulf (1986) using monochromated synchrotron radiation, the linear form for the scan-range formula has been queried by Mathieson (1988), attention being drawn to the possibility that, in such situations, a different, root mean square (RMS), form of relationship is more appropriate, namely $\omega = [(p)^2 + (q \tan\theta)^2]^{1/2}$ or, with a monochromator crystal M, $[(p')^2 + \langle q'(t - t_{\min})\rangle^2]^{1/2}$ where $t = \tan\theta/\tan\theta_M$ and $t_{\min}$ corresponds to the condition of minimum wavelength dispersion.

Despite the long history of profile measurement, the possibility that particular functional forms for the scan range formula are allied to different shapes of Bragg reflection profiles and, consequently, influenced by the shapes of their constituent components does not appear to have been examined previously. This possibility would appear to be a matter of some interest for the procedural details of 1D measurement when 'best' results are sought, *e.g.* in deformation electron density studies.

Relevant features of reflection profiles

Truncation

For the estimation of the integrated intensity of single-crystal Bragg reflections, theory implies that integration should extend to infinity. Indeed, underlying the conventional approach to the measurement procedure is the assumption that the scan width is sufficient to ensure that every reflection is fully contained within the central measurement points (*e.g.* Clegg, 1984). For any practicable experimental procedure, this is clearly impossible; see, for instance, Fig. 1 of Dam, Harkema & Feil (1983). Some realistic restriction (truncation) on the $\Delta\omega$ range [and the $\Delta 2\theta$ (aperture) range, where necessary] must be set. Once decided upon, these limits have to be maintained in such a way as to ensure that measurements on all reflections are placed on the same basis and hence yield comparable values of integrated intensity.

The limits within which the signal intensity is ascribed to the Bragg reflection and outside which it is used for correctional background estimation constitute the truncation limits. What one requires to aim for is to establish truncation limits which are consistent as one moves from reflection to reflection. The magnitude of the systematic errors which arise from failure to adjust the scan range to maintain consistent truncation have been examined theoretically, but only within the context of the linear form, by Denne (1977*a*, *b*), for the case of an α_1, α_2 doublet. He devised a correction formula which has been tested with varying results by several authors [see references in Destro & Marsh (1987)].

Under conditions of non-consistent truncation, one is, in fact, transposing part of the 'peak' into 'background' or *vice versa* and so modifying the balance or ratio between these two regions in such a relatively ill-defined manner that the subsequent numerical correction may not be able to provide appropriate compensation. It follows that incorrect truncation may introduce errors of a systematic but not readily identifiable nature. If, however, one can achieve the conditions for consistent truncation, then the subdivision into 'peak' and 'background' is maintained constant as also will be the subtraction of 'background' from 'peak'. Even if other factors obtrude, such as thermal diffuse scattering, the maintenance of a consistent region in diffraction space for intensity measurement ensures a basic compatibility of reflections.

Given that, in principle, we are after consistent truncation, we need to consider what we mean by it in operational terms, how we aim for it and how we ascertain that we are, in fact, achieving that goal.

General features of a Bragg reflection

We need first to consider the general features of any single peak 'counter' 1D profile. Firstly, it has a maximum value, secondly, we can give a figure to its width at half maximum (WHM) and, thirdly, it has a width at its base. Since this last is in the region where signal is becoming indistinguishable from noise, this is the least straightforward feature to establish. Nevertheless, it is the truncation limits corresponding to this width which we must attempt either to identify or, at least, be able to set on a rational basis.

First, we need to gain insight into these diagnostic features by examining a number of models involving different functional forms for the components which, convoluted together, generate the profile.

Models

Singlet wavelength peak case

Consider the basic situation involving two components, one invariant with respect to θ [say, the source emissivity, $\sigma(= a)$, but it could include other

invariant components], and the other, functionally dependent on θ, corresponding to the wavelength dispersion, λ, of the singlet peak ($= b \tan \theta$).

In 2D $\Delta\omega$, $\Delta 2\theta$ space, the situation is shown in Fig. 1(a) for (i) square wave, (ii) trapezoidal and (iii) Gaussian components.

Projection of these 2D distributions onto the $\Delta\omega$ axis yields the profile shapes (Fig. 1b), which also correspond to the convolution of the projections on ω of the components σ and λ respectively (see Alexander & Smith, 1962). It is of interest to examine how these cases change over a range of θ, from small to large. The integral of the λ distribution with change in θ is held constant in any one situation.

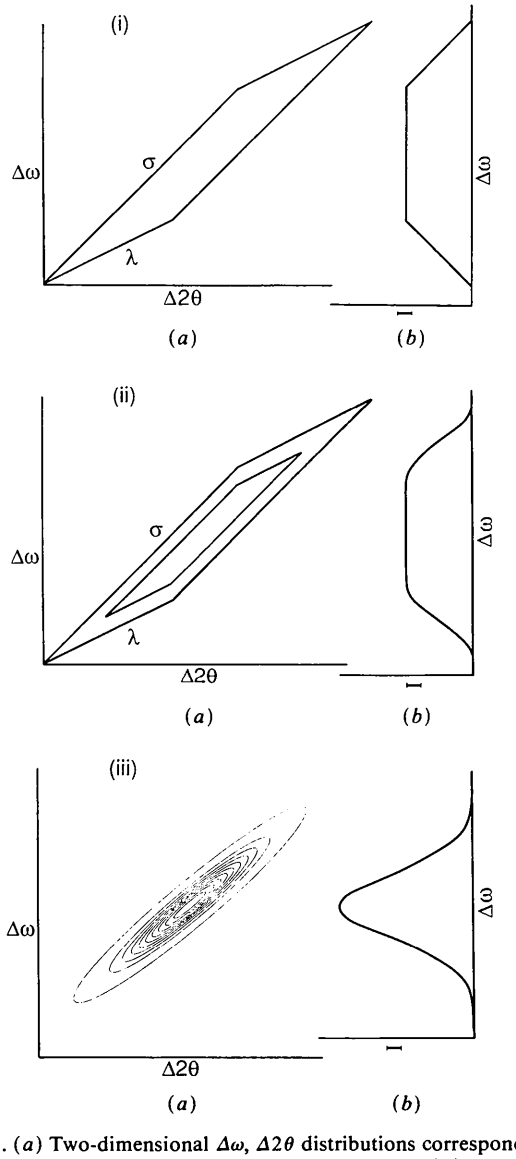

Fig. 1. (a) Two-dimensional $\Delta\omega$, $\Delta 2\theta$ distributions corresponding to the convolution of a θ-invariant component (σ) and a θ-variant component (λ) for (i) square wave, (ii) trapezoidal and (iii) Gaussian components. (b) The corresponding one-dimensional profiles derived by projection along $\Delta 2\theta$.

For square-wave components at low angles, *i.e.* when $b \tan \theta < a$, the convoluted result has a base $(a + b \tan \theta)$, a plateau width of $(a - b \tan \theta)$ and a width at half maximum (WHM) of a. For larger scattering angles, as the magnitude of $b \tan \theta$ reaches that of a, the shape becomes triangular and subsequently the WHM becomes $b \tan \theta$ while the width at the base remains $(a + b \tan \theta)$. In other words, the functional relationship of the base is $(a + b \tan \theta)$ while that of the WHM is first constant and then rises linearly with increase in θ.

Where the shapes of the components are trapezoidal, Fig. 1(ii), the projected results have similarities to those for square waves. If the λ (or $b \tan \theta$) function is reduced to a delta function, then the result is the same as in Fig. 1(i). With the $b \tan \theta$ function larger but still less than the σ function, the result is a somewhat rounded figure, with the base width a linear combination of the base widths of the two components. The WHM corresponds to the WHM of the larger component, namely a (σ). The peak plateau width is dependent on the side slopes of the two components σ and λ.

When the two components are each Gaussian in shape, Fig. 1(iii), the convoluted 1D resultant is, of course, Gaussian, the peak being single valued. The WHM is $[(p)^2 + (q \tan \theta)^2]^{1/2}$ irrespective of whether p or $q \tan \theta$ is the greater (p and $q \tan \theta$ are the WHM of the individual components). The base is theoretically infinite but if one defines a practical outer limit as (say) 0·01 (or 0·001) of the peak value then the base corresponds to $n \times$(WHM) [or $m \times$(WHM)] where $n = 2{\cdot}578$ and $m = 3{\cdot}157$. On this basis, the appropriate scan range would therefore be of the form $[(p')^2 + (q' \tan \theta)^2]^{1/2}$ where $p' = np$ (or mp) and $q' = nq$ (or mq). The decision here as to the scan range is in fact more straightforward than for rectilinear shapes in that it can be set in terms of the (observable) WHM.

Although the simple combination of two Gaussians is likely to apply only in special cases, *e.g.* with monochromated synchrotron radiation (Mathieson, 1988), it is nevertheless of interest to consider this situation and compare the consequent scan range involving the RMS form with that for the conventional linear form. For this purpose, we set up a series of synthetic 1D profiles composed of a non-dispersive Gaussian component [source (say)] convoluted with a single-peak dispersive Gaussian component (wavelength) for values of $k \tan \theta$ from 0 to 1·0 in steps of 0·1. The profiles of the latter component are normalized to the same integral value so that all convoluted profiles have the same integral (to infinity). (The value of k in practice would vary with the range of θ in the particular experimental set up.) The scan range values corresponding to the RMS relationship are determined where the profile ordinates drop to (say) 1% of the convoluted peak, this

Table 1. *Scan ranges*

$k \tan \theta$	ω_{LIN}	ω_{RMS}	$\omega_{LIN}/\omega_{RMS}$	I_{LIN}	I_{RMS}	I_{LIN}/I_{RMS}
0·0	0·6	0·6	1·0	97·615	97·615	1·0
0·1	0·8	0·6928	1·1547	99·441	97·615	1·0187
0·2	1·0	0·9165	1·0911	98·957	97·615	1·0138
0·3	1·2	1·20	1·0	97·615	97·615	1·0
0·4	1·4	1·510	0·9272	95·651	97·615	0·9799
0·5	1·6	1·8330	0·8729	93·425	97·615	0·9571
0·6	1·8	2·1633	0·8321	91·205	97·615	0·9343
0·7	2·0	2·4980	0·8006	89·121	97·615	0·9130
0·8	2·2	2·8355	0·7759	87·231	97·615	0·8936
0·9	2·4	3·1749	0·7559	85·527	97·615	0·8762
1·0	2·6	3·5157	0·7395	84·020	97·615	0·8607

choice being arbitrary and selected merely for demonstration. The resultant values are shown in Table 1 and yield the curve in Fig. 2(*a*). Since we presume that we are treating some quasi-realistic situation, the scan-range curve corresponding to the linear relationship should cross the RMS curve at some intermediate point in the range. We have arbitrarily chosen this to be $k \tan \theta = 0{\cdot}3$. The resultant scan-range values corresponding to the linear relationship are also given in Table 1 and yield the straight line in Fig. 2(*a*). Below $k \tan \theta = 0{\cdot}3$, it is evident that the RMS scan range would be less than that due to the linear scan range, while above $k \tan \theta = 0{\cdot}3$ it would be greater and progressively so as θ increased.

Following the conventional procedure for determining the total peak intensity (P) between the scan-range limits, the background estimate (B) from the ordinates at the scan-range limits and the abscissa between the scan-range limits, the integrated intensity being ($P - B$), estimates of the integrated intensity of the series of synthetic profiles were made at the 1% level for both the RMS and the linear cases (see Table 1).* The estimates for the RMS scan relationship are constant with change in θ while those for the linear form are initially larger and then progressively smaller. The trend I_{LIN}/I_{RMS} *versus* $k \tan \theta$ is indicated in Fig. 2(*b*).

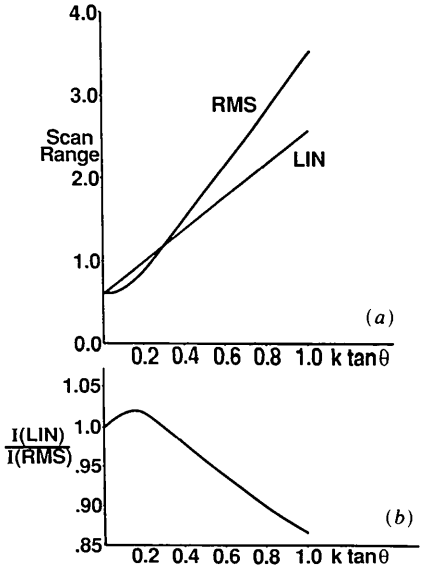

Fig. 2. (*a*) Plots of a scan-range variation with $k \tan \theta$ corresponding to the linear formula, and to the RMS formula, coincident at $\theta = 0°$ and at the cross-over point, $k \tan \theta = 0{\cdot}3$. (*b*) Plot of the ratio I_{LIN}/I_{RMS} *versus* $k \tan \theta$.

It must be stressed that the synthetic data treated above are intended purely for illustration of the trend associated with use of the linear relationship rather than the RMS relationship in situations which can be modelled essentially by Gaussians for both the non-dispersive and dispersive components.

In many laboratory experimental arrangements, the distribution representing the source emissivity cannot be represented by a single Gaussian but involves a plateau, like Fig. 1(ii). For this combination, the appropriate scan-range formula involves a RMS component, p', from the convolution of the Gaussian defined by the leading and trailing edges of the source distribution and q' from the wavelength dispersion, plus a linear component, p'', from the displacement component of the source emissivity.

$$\omega = [(p')^2 + (q' \tan \theta)^2]^{1/2} + p''. \qquad (1)$$

In such cases, the curve determining the scan range will lie between the RMS and the linear form. The curvature trend illustrated in Fig. 2 will still apply but will be less extreme.

Lorentzian peaks

So far the peaks or peak components have been discussed in terms of Gaussian shapes. While this may be a valid approximation for some beams monochromated by reflection from an extended-face crystal, the shapes of characteristic lines are known to be Lorentzian. How does this affect the scan range?

If the effective abscissa range of the Lorentzian is large, *i.e.* effectively infinite, then the convolution of two Lorentzians is such that the WHM of the resultant corresponds to the sum of the WHMs of the individual components, which would correspond to a linear relationship for the scan range. If, however, the abscissa range is restricted, for example by apertures or monochromatization, then the WHMs will tend to combine in a manner closer to RMS fashion.

Doublet wavelength peak case

In the case of commonly used characteristic X-ray sources, these are generally doublet in character, α_1, α_2. This means that the separation of the two peaks, $(\Delta\lambda/\lambda) \tan \theta$ $(= q'')$, has to be taken into

* It is recognized that use of the Gaussian profile curve without normal 'noise' background is a gross simplification and is utilized simply to reveal the form of difference resulting from the truncation formulae.

account. As we have noted above, the separation of the peaks makes a linear contribution to the scan range. This does not take account of the 'natural' widths of the two peaks outside the peak separation (see Alexander & Smith, 1962; Burbank, 1964; Mathieson, 1984*b*).* If these edges can be modelled as Gaussian then their contribution, q', will be a RMS component.

As a result, the formula appropriate to this situation is

$$\omega = [(p')^2 + (q' \tan\theta)^2]^{1/2} + (p'' + q'' \tan\theta). \quad (2)$$

In the case of (say) Mo $K\alpha_1\alpha_2$, the line widths at half height are $0{\cdot}29\times10^{-3}$ Å (α_1) and $0{\cdot}32\times10^{-3}$ Å (α_2) with the $\alpha_1\alpha_2$ separation being $4{\cdot}28\times10^{-3}$ Å. While these line widths at HM are small relative to the $\alpha_1\alpha_2$ separation, their contribution to scan range depends on the point at which truncation is assumed to occur (n times the WHM). In the terms of Mathieson (1984*b*), q' would correspond to twice the $\alpha_1\alpha_2$ separation and q'' to the $\alpha_1\alpha_2$ separation.

The appropriate weights of the RMS and linear components in (2) are dependent on the particular experimental parameters, including those of the specimen crystal and, for best results, these require to be established in each experiment.

Provided that one is only concerned with the general curvature trend with θ, one can use an approximation, $\omega = [(c)^2 + (d \tan\theta)^2]^{1/2}$, but then the terms c and d no longer have direct physical significance.

Comparison with the measurement data of Eisenstein & Hirshfeld (1983)

In virtually all published structure analyses, the effects of truncation have not been recognized as such and have been absorbed in least-squares refinement, mainly by the thermal parameters. Where recognized, they have been corrected by use of the Denne (1977*a*) formula which, as Denne showed, has effects similar to a temperature-factor contribution. The basic problem with the least-squares procedure is that it operates only in relation to recognized, and therefore included, factors. It cannot identify an unspecified factor but accommodates it within one or more of the nominated factors. So it is not easy to get hold of recorded experimental data which can be used to test the conclusions in the present paper.

The work of Eisenstein & Hirshfeld (1983) has the rare distinction that it involved a careful analysis of the measurements of the individual reflection peaks and background and presented these in summary form as average changes over specified variables. In addition, there was no attempt to obscure the existence of their idiosyncratic variation with θ which became evident. The authors stated frankly that, in their view, 'no plausible truncation model could account for this behaviour'. As a result, they provide a unique (in the proper sense of the word) set of measurements which are uncorrected for truncation and, having been recorded at liquid N_2 temperature and therefore relatively extensive in θ, are consequently ideally suited to allow test of the deductions presented here.

As part of their data analysis, Eisenstein & Hirshfeld derived essentially the ratio of F_o/F_c for groups of reflections with increasing θ. The result was unexpected and was described in their words as follows: 'Up to $\theta \sim 35°$, the ratio lay in the region 1·03, then it dipped rapidly to a minimum of 0·92, *ca* $\theta = 60°$. After this, it rose to values above 1·11.' (Maximum θ was *ca* 76°.) We have taken the liberty of sketching this trend in Fig. 3 as a function of θ and as a function of $(1/2)\tan\theta$.

If one compares Fig. 3(*b*) with Fig. 2(*b*), there is a close parallel in respect to the trends, up to $\theta = 60°$ in Fig. 3(*b*). Basically, the discrepancy is positive to *ca* $\theta = 35°$ then goes negative to $\theta = 60°$, the cross-over point being in the region $\theta = 30$–$35°$. We therefore conclude that, for the region $\theta = 0$ to 60° (which constitutes the major intensity weight of the data and hence dominates the resultant deformation density), the discrepancy between F_o and F_c rests essentially

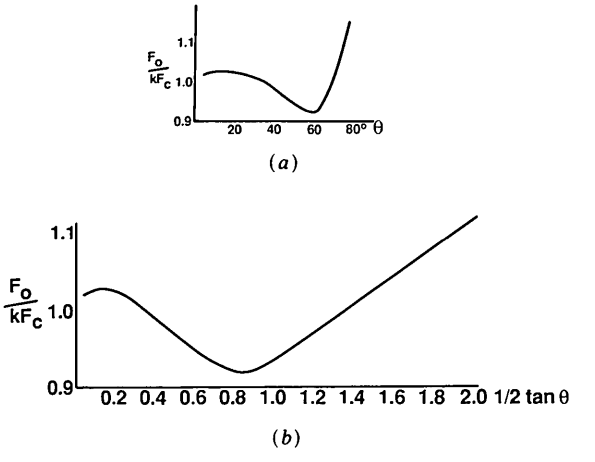

Fig. 3. Sketch of the idiosyncratic relationship of the ratio F_o/F_c described by Eisenstein & Hirshfeld (1983) (*a*) *versus* θ and (*b*) *versus* $(1/2)\tan\theta$.

* In the series of studies by Hope & Hirshfeld and their associates, namely Hope & Ottersen (1978), Ottersen & Hope (1979), Eisenstein (1979), Hirshfeld & Hope (1980), Ottersen, Almhof & Hope (1980), Ottersen, Almhof & Carle (1982), Eisenstein & Hirshfeld (1983) and the study by Destro & Marsh (1987), the wavelength dispersion component was set as the angular separation of $\alpha_1\alpha_2 = S°$. This meant that no account was taken of the contribution of the leading and trailing edges of the doublet lines (*cf.* Alexander & Smith *etc.* above). Note, however, that, although Eisenstein & Hirshfeld (1983) made measurements with $(1{\cdot}2+1{\cdot}5S)°$, their integrated intensity estimates were based on the range $(0{\cdot}8+S)°$.

with the measurement of F_o and is due to the use of a linear formula rather than a RMS formula for the scan range.

There still remains the trend with θ from *ca* 60 to 76°. It seems evident that this is due to an additional factor not directly allied to truncation. Eisenstein & Hirshfeld supply evidence which may be indicative. With their careful examination of their reflection data they found that there 'was a linear dependence of the apparent background on the associated reflections, due to the intrusion of the Bragg reflections into the "background" regions. But, contrary to the expected behaviour, the shape of the dependence was found to reach a maximum near $\theta = 70°$ and to decrease at higher values of θ.' In this context, one should note also the indicator of change in the direction of the curve in Fig. 1(*a*) of Eisenstein & Hirshfeld from *ca* 60° onward. The overall evidence tends to confirm the cause of this trend of F_o/F_c as involving a feature not significantly obvious in the region below $\theta = 60°$. It would appear that it involves a scattering process which can contribute to the Bragg peak but does not obtrude into the region normally classed as background, so that, with increase in θ, $P - B$ (as assessed normally) is increasing while B/P is decreasing. This matter is treated further under *Discussion*.

If these features are the basis for an explanation of the idiosyncratic plot of F_o/F_c, it is clear that the original temperature parameters, derived without the application of appropriate corrections, are likely to be questionable, as Eisenstein & Hirshfeld observe, and it may be that resultant errors in temperature factors contribute to the shape of the F_o/F_c curve at higher θ.

Discussion

From this examination, it is evident that accurate estimation of structure-factor values from single-crystal Bragg reflection 1D profiles is dependent not only on experimental care in the measurement operations but also on a proper recognition of the theoretical basis of the operations involved and of the specific experiment under way. It is therefore somewhat surprising to realize that the basic question of the relationship between the formula for the scan range and the specific shapes of the components which, convoluted together, establish the profile shape, has received no attention during the long annals of this measurement procedure; one which is basic to the derivation of integrated intensities and structure factors.* The present exercise, primitive as it is, shows clearly that the conventional linear formula for determining scan range is to be associated essentially with components whose shapes are such that the integral is operationally to infinity. It also shows that, for 'rounded' (Gaussian) components with a finite mean square width, a RMS formula is more appropriate. Since the majority of shapes of components involved in diffraction experiments are mainly of the rounded type, it would appear that an appropriate mixture of RMS and linear should be used in practice. Only if it is established experimentally that the scan range truly encompasses the whole reflection is the linear form appropriate.

It has been shown above (Fig. 2*b*) that if one restricts oneself to a linear formula for scan range where a RMS formula is actually appropriate, it can lead to two regions of opposite effect on the integrated intensity estimate, below and above the cross-over value of θ. In the past it was assumed that the effect started at $\theta = 0°$, *i.e.* the cross-over point coincided with $\theta = 0°$ and was always in one direction - to reduce the intensity measured. Historically, the potential effect of truncation errors was identified by Alexander & Smith (1962) and discussed by them and subsequently by others (*e.g.* Ladell & Spielberg, 1966; Kheiker, 1969; Young, 1969; Werner, 1971, 1972; Einstein, 1974). However, in practice, correction for this error source was largely ignored by structure analysts. It was in relation to an ω/θ scan-mode monochromatization technique that Denne (1977*a*, *b*) derived a correction formula for the effect of truncation on the basis of a linear scan-range formula, assuming thereby that the effect was progressive from $\theta = 0°$. In a low-temperature study, Hope & Ottersen (1978) noted a systematic trend of the ratio F_o/F_c with increasing θ angle which they ascribed to this form of truncation. They therefore used Denne's formula to apply corrections. Thereafter, Hope and co-workers and Hirshfeld and co-workers used Denne's correction procedure in their deformation studies. While generally the situation was improved, they observe that, in some cases, the correction may have been insufficient. As discussed above, Eisenstein & Hirshfeld (1983) came to the conclusion that their data had a strange θ dependence not correctable by use of the Denne formula while Destro & Marsh (1987) tested Denne's formula but found it inadequate and devised their own procedure. Even so, they had to invoke an additional θ-dependent 'aberration function' to achieve a match of experimental and theoretical profiles. No details of the form of the 'aberration functions' were given.

The present study offers a resolution of the difficulty by showing that the scan-range formula should be more complex than the simple linear formula and that, with this approach, one should be able to establish a rational procedure for measurement which provides for consistency over the operational range of θ.

Failure to use a correct formula for scan range can have an effect not only on derived temperature factors

* While it true that 'profile fitting' has been explored (*cf.* Clegg, 1981), in general this has been based on an *ad hoc* approach and, while not always specified, has relied essentially on the applicability of the linear scan-range relationship.

mainly associated with the high-angle region but also on parameters for extinction mainly associated with the low-angle region. If, due to the use of a linear formula, the scan range in the low-θ region is larger than it should be (see Fig. 2*a*), then the resultant estimates of integrated intensity and structure factors are affected similarly. As a result, the full effect of extinction on strong reflections in that region will be partially concealed (see also Mathieson, 1984*a*) and so the magnitude of correction for extinction will be underestimated.

With computer control of diffractometers, there should be no difficulty in applying an appropriate mix of RMS and linear components to set the proper scan range with alteration of θ. However, the establishment of the required basic experimental parameters will necessitate careful measurement. Probably the most straightforward approach is by measurement of $\Delta\omega, \Delta 2\theta$ distributions for a number of selected reflections (Mathieson, 1982). Such measurements would provide estimates of the individual component distributions - source and mosaic spread - while the wavelength distribution for the particular radiation can be established from published sources or derived from the $\Delta\omega, \Delta 2\theta$ distributions (*e.g.* Mathieson, 1984*b*).

Burbank (1964) drew attention to a subtle feature of profile measurement which is associated with its generation by the convolution of various components. As the wavelength dispersion changes with θ, the contributions from the wavelength band to the convoluted profile can change with the change in scan range so that the profile integrated intensity, considered on a normalized basis, can change in magnitude with θ, thus introducing a systematic error. Burbank notes that, according to this argument, one can only be certain of the wavelength band being constant if one uses balanced filters. The present analysis offers an alternative view concerning profile measurement. If the scan range is properly adjusted, the integrated intensity within the scan range is maintained constant with change in dispersion, on a normalized basis (see Table 1, column 6). The possibility of treating data collection in terms of bands with different but internally consistent scan ranges and using common reflections for interpolation has been mentioned earlier (Mathieson, 1982).

A possible clue as to an explanation for the F_o/F_c curve above $\theta = 60°$ may be derived from a study by Ohba, Sato, Saito, Ohshima & Harada (1983). They found that their estimates of certain high-angle F_o's were generally greater than the corresponding F_c's and, after eliminating TDS as the source of the discrepancy, they concluded that Huang scattering was the probable cause of the difference. In general, Huang (1947) scattering is associated with a reduction of the Bragg peak and an increase in diffuse scattering adjacent to the Bragg peak which would produce an effect opposite to that observed. However, if the Huang scattering is markedly anisotropic (due to anisotropic strains) then a certain proportion of the reflections could be observed to have a greater diffuse contribution close under the Bragg profile and a lesser contribution in the background region [see Fig. 2 of Harada (1988)]. In the lower-θ region, the population of reflections would be such that, on average, the Huang scattering would constitute a contribution to both peak and background regions. As one progresses into the higher-θ region, the population of observable reflections drops away rapidly so that it is only the more intense reflections with lesser background that are measured. It is presumably these that contribute to the marked change in the ratio B/P recorded by Eisenstein & Hirshfeld.

In the case of Eisenstein & Hirshfeld, the data were collected at liquid-N_2 temperature so the role of TDS would be minor while extra diffuse scattering from lattice defects (possibly produced and 'locked in' by the original cooling process) would not of course be reduced by the low temperature of the specimen.

So we conclude that the evidence points to two causes for the discrepancies in the Eisenstein & Hirshfeld data. The main one, principally affecting the lower-angle region, is due to the use of a linear scan-range formula rather than a RMS formula while the other, more significant at higher angles but less significant in gross magnitude, is ascribed to the selective effect of Huang scattering. The two effects overlap and, particularly in the higher region, change their balance with one going negative and the other going positive, leading to the gross swings in the region $\theta = 50$ to 76°.

I am greatly beholden to Dr J. K. Mackenzie for the convolution program and for much discussion on various aspects of this paper and to Dr A. W. Stevenson for the plot of the ellipse, and to both for their helpful suggestions on the text. Any misinterpretations arising from such discussion are however wholly my responsibility.

References

ALEXANDER, K. E. & SMITH, G. S. (1962). *Acta Cryst.* **15**, 983-1004.
ARNDT, U. W. & WILLIS, B. T. M. (1966). *Single Crystal Diffractometry.* Cambridge Univ. Press.
BURBANK, R. D. (1964). *Acta Cryst.* **17**, 434-442.
CLEGG, W. (1981). *Acta Cryst.* **A37**, 22-28.
CLEGG, W. (1984). *Methods and Applications in Crystallographic Computing*, edited by S. R. HALL & T. ASHIDA, pp. 30-40. Oxford: Clarendon Press.
DAM, J., HARKEMA, S. & FEIL, D. (1983). *Acta Cryst.* **B39**, 760-768.
DENNE, W. A. (1977*a*). *Acta Cryst.* **A33**, 438-440.
DENNE, W. A. (1977*b*). *Acta Cryst.* **A33**, 987-992.
DESTRO, R. (1988). *Aust. J. Phys.* **41**, 503-510.
DESTRO, R. & MARSH, R. E. (1987). *Acta Cryst.* **A43**, 711-718.
EINSTEIN, J. R. (1974). *J. Appl. Cryst.* **7**, 331-344.

EISENSTEIN, M. (1979). *Acta Cryst.* B**35**, 2614-2655.
EISENSTEIN, M. & HIRSHFELD, F. L. (1983). *Acta Cryst.* B**39**, 61-75.
HARADA, J. (1988). *Aust. J. Phys.* **41**, 351-357.
HIRSHFELD, F. L. & HOPE, H. (1980). *Acta Cryst.* B**36**, 406-415.
HÖCHE, H. R., SCHULZ, H., WEBER, H.-P., BELZNER, A., WOLF, A. & WULF, R. (1986). *Acta Cryst.* A**42**, 106-110.
HOPE, H. & OTTERSEN, T. (1978). *Acta Cryst.* B**34**, 3623-3626.
HUANG, K. (1947). *Proc. R. Soc. (London) Ser. A.* **190**, 102-117.
KHEIKER, D. M. (1969). *Acta Cryst.* A**25**, 82-88.
LADELL, J. & SPIELBERG, N. (1966). *Acta Cryst.* **21**, 103-122.
MATHIESON, A. MCL. (1982). *Acta Cryst.* A**38**, 378-387.
MATHIESON, A. MCL. (1983). *J. Appl. Cryst.* **16**, 572-573.
MATHIESON, A. MCL. (1984*a*). *Acta Cryst.* A**40**, 355-363.
MATHIESON, A. MCL. (1984*b*). *Aust. J. Phys.* **37**, 55-61.
MATHIESON, A. MCL. (1988). *Acta Cryst.* A**44**, 239-243.
MATHIESON, A. MCL. & STEVENSON, A. W. (1985). *Acta Cryst.* A**41**, 290-296.
OHBA, S., SATO, Y., SAITO, Y., OHSHIMA, K.-I. & HARADA, J. (1983). *Acta Cryst.* B**39**, 49-53.
OTTERSEN, T., ALMHOF, J. & CARLE, J. (1982). *Acta Chem. Scand. Ser. A*, **36**, 63-68.
OTTERSEN, T., ALMHOF, J. & HOPE, H. (1980). *Acta Cryst.* B**36**, 1147-1154.
OTTERSEN, T. & HOPE, H. (1979). *Acta Cryst.* B**35**, 373-378.
WERNER, S. A. (1971). *Acta Cryst.* A**27**, 665-669.
WERNER, S. A. (1972). *Acta Cryst.* A**28**, 143-151.
YOUNG, R. A. (1969). *Acta Cryst.* A**25**, 55-66.

Acta Cryst. (1989). A**45**, 620-628

High-Voltage Electron Diffraction from Bacteriorhodopsin (Purple Membrane) is Measurably Dynamical

BY R. M. GLAESER

Biophysics Department and the Donner Laboratory, Lawrence Berkeley Laboratory, University of California, Berkeley, CA 94720, *USA*

AND T. A. CESKA

NRC Biotechnology Research Institute, 6100 *Royalmount Ave, Montreal, Quebec, Canada H4P 2R2*

(*Received* 7 *November* 1988; *accepted* 7 *April* 1989)

Abstract

Electron diffraction patterns of 45 Å thick two-dimensional crystalline arrays of a cell membrane protein, bacteriorhodopsin, have been recorded at two electron voltages, namely 20 and 120 kV. Significant intensity differences are observed for Friedel mates at 20 kV, but deviations from Friedel symmetry are quite small at 120 kV. It does not seem likely that the measured Friedel differences can be accounted for by complex atomic structure factors, by curvature of the Ewald sphere, or by effects that might occur as a result of inelastic scattering (absorption). It is therefore concluded that dynamical diffraction within the single molecular layer of these crystals is responsible for the observed Friedel differences. The results are useful in estimating the maximum specimen thickness for which the kinematic approximation may be safely used in electron crystallography of biological macromolecules at the usual electron voltage of 100 kV, or even at higher voltages. The results show that the Friedel differences are independent of resolution and this opens up the possibility that dynamical effects occurring at lower voltages might be used to phase higher-voltage kinematic diffraction intensities.

Introduction

Bacteriorhodopsin is a protein of molecular weight 27 000 which naturally forms well ordered monolayer crystals within the cell membrane of *Halobacterium halobium.* These crystalline patches, known as purple membrane, are readily isolated from the bacteria as small membrane fragments only 45 Å thick (Blaurock, 1975; Henderson, 1975) and typically 0·3 μm^2 in area. Single-crystal X-ray diffraction patterns cannot be measured from these specimens because of the small size of the purple membrane fragments. Electron diffraction and high-resolution electron microscopy therefore represent the method of choice for a crystallographic structure analysis of the constituent protein, bacteriorhodopsin. Progress in this structure analysis, which includes a three-dimensional density map at 6 Å and a two-dimensional projection at 3·5 Å resolution, has been reviewed by Baldwin, Ceska, Glaeser & Henderson (1987).

The use of electron diffraction and high-resolution image data to produce Coulomb potential density maps has so far assumed that the electron-specimen interaction can be described to a satisfactory degree of accuracy by the weak-phase-object (WPO) approximation (Hoppe, 1970; Erickson, 1974; Amos, Henderson & Unwin, 1982). The WPO approximation is a simplified version of the single-scattering kinematic approximation, in which the Ewald sphere is approximated as a plane (Glaeser, 1985). Other factors that are ignored in the WPO approximation, but which can affect the experimental data, include

0108-7673/89/090620-09$03.00